Supporting information

Unusual Conversion-type Lithiation in LiVO$_3$ Electrode for Lithium-Ion Batteries

Jeong Beom Lee,[†] Janghyuk Moon,[‡] Oh B. Chae,[†] Jae Gil Lee,[†] Ji Heon Ryu,[§]

Maenghyo Cho,[‡] Kyeongjae Cho,[‖] and Seung M. Oh[*,†]

[†]Department of Chemical and Biological Engineering and Institute of Chemical Processes and [‡]WCU Multiscale Mechanical Design Division, Department of Mechanical and Aerospace Engineering, Seoul National University, 1 Gwanak-ro, Gwanak-gu, Seoul 08826, Republic of Korea

[§]Graduate School of Knowledge-based Technology and Energy, Korea Polytechnic University, 237 Sangidaehak-ro, Siheung-si, Gyeonggi 15073, Republic of Korea

[‖] Department of Materials Science and Engineering and Department of Physics, The University of Texas at Dallas, Richardson, Texas 75080, United States

[*]Corresponding author: Tel.: +82-2-880-7074

E-mail address: seungoh@snu.ac.kr (S. M. Oh)

Computational details

LiVO$_3$ and Li$_2$VO$_3$ structures were extracted from ICSD database, and the other structures were generated by inserting Li$^+$ ions into the basic structures. The detailed procedure is as follows.

The structure of synthesized material was confirmed by XRD measurement. (Figure S3) It is LiVO$_3$ (JCPDS no. 33-0835) which belongs to $C2/c$ space group. The same structure was found in ICSD database (ICSD-68634) and geometric relaxation was performed. Since the LiVO$_3$ phase loses its long-range order during lithiation as seen on the *ex-situ* XRD pattern (Figure S4), the intermediate phases were predicted based on the results reported by Pralong *et al.* (*Chem. Mat.*, **2012**, *24*, 12-14) and electrochemical (Figure 2) and spectroscopic data (Figure 3, 4).

However, the structure of Li$_2$VO$_3$ is not known. Hence, the possible candidate structures were selected from the Li$_2$[TM]O$_3$ series in the ICSD database and double-checked by using the crystal prediction module provided by Materials Project. The candidate structures were further narrowed down by considering the experimental data, which suggests V^{4+} ions in octahedral sites. After all the candidates were relaxed using DFT calculation (Table S1), the most stable one was extracted, which has Li$_2$MnO$_3$ structure (ICSD-46953).

All the structure and reaction potential prediction were executed based on the experimental results. The modeling of lithiation in the LiVO$_3$ (Stage A) was performed as follows. One Li$^+$ ion was added into the interstitial sites or vacancies existing in 2 × 1 × 1 cell of LiVO$_3$ (contains 8 Li$^+$ ions) and the structures were relaxed using DFT calculation to find the most stable one. The same procedure was repeated until 8 Li$^+$ ions were inserted into the 2 × 1 × 1 cell of LiVO$_3$ to generate Li$_2$VO$_3$. Li$^+$ extraction in 2 × 1 × 1 cell of Li$_2$VO$_3$ structure was also performed. The formation energy was calculated using the following equation.

$$\Delta E_f = E_f(\text{Li}_y\text{VO}_3) - [E_f(\text{Li}_x\text{VO}_3) + (y-x)E_f(\text{Li})]$$

The formation energies of Li$_{1+x}$VO$_3$ (0 < x < 1) (single-phase reaction) were then compared to

1

that of the two-phase reaction between $LiVO_3$ and Li_2VO_3. As seen in Figure S5a, the formation energies for the single-phase reaction show larger value than that of two-phase reaction, implying that the two-phase reaction is thermodynamically favored. The voltage plateaus obtained from the calculated formation energies were determined by convex hull theorem. The reaction potential during lithiation was calculated using the following equation.

$$V = -\frac{\Delta E_f}{(y-x)F}$$

The lithiation in Li_2VO_3 was performed in the same way. Li^+ ion was inserted into the interstitial sites or vacancies existing in $2 \times 1 \times 1$ cell of Li_2VO_3 (contains 16 Li^+) and the geometry relaxation was performed. To simulate the amorphous structure of $Li_{2+x}VO_3$, Molecular Dynamics (MD) simulation (T = 1200 K) was performed. The layered structure of Li_2VO_3 maintains until the 8 Li^+ addition. However, the layered structure starts to collapse after $Li_{2.5}VO_3$ (x = 1.5); after all the possible interstitial site are occupied by Li^+ ions. Further lithiation was simulated by continuously adding Li^+ ions into the largest void space by Delaunay triangulation method. The structures were then MD simulated and relaxed repeatedly. Finally, after 5 Li^+ addition into $LiVO_3$, the vanadium metal cluster and Li-O cluster can be obtained.
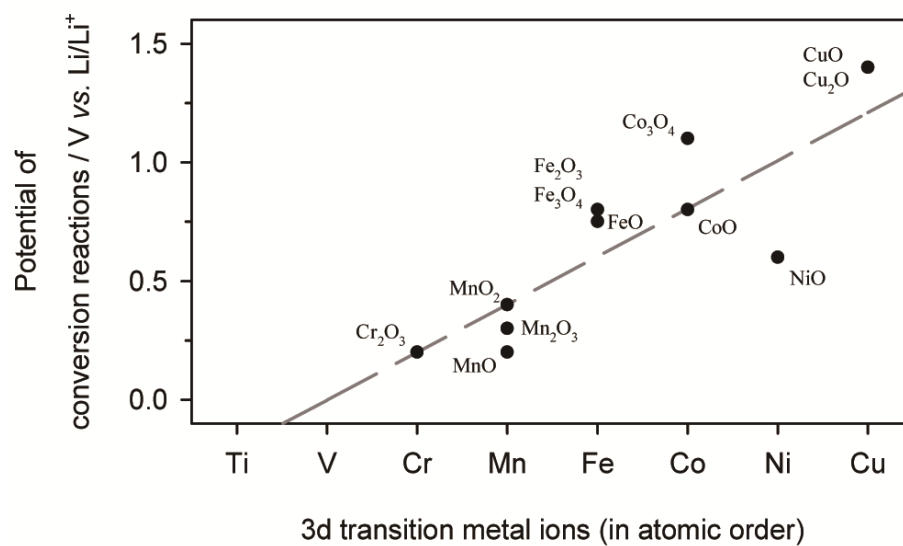
Figure S1. The empirical values and their regression curve of conversion plateau of 3d transition metal oxides.[1]

Reference

(1)   Cabana, J.; Monconduit, L.; Larcher, D.; Palacín, M. R. Beyond Intercalation-Based Li-Ion Batteries: The State of the Art and Challenges of Electrode Materials Reacting through Conversion Reactions. *Adv. Mater.* **2010**, *22* (35), E170–E192.
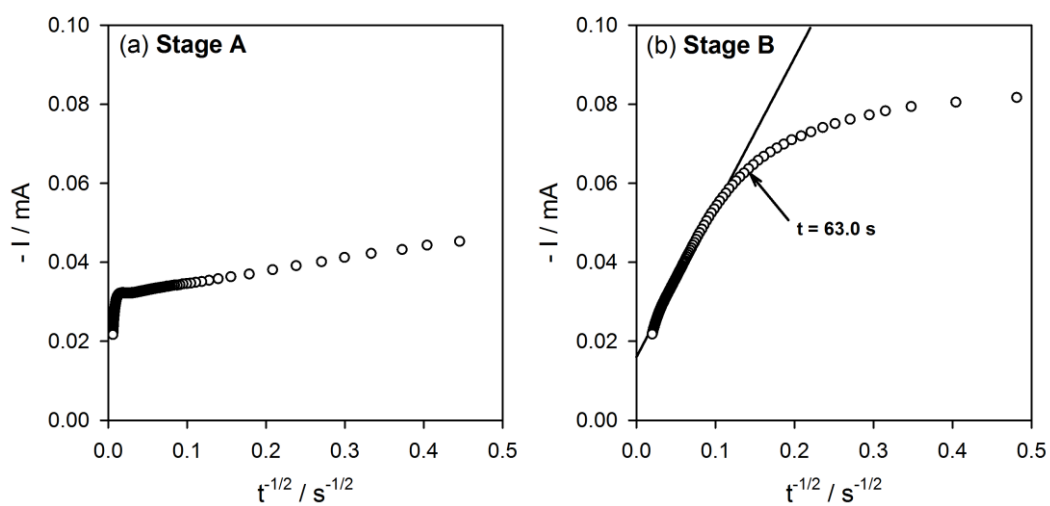
Figure S2. Current versus t$^{-1/2}$ plots for the current transient in stage *A* and *B* obtained from PITT measurement.
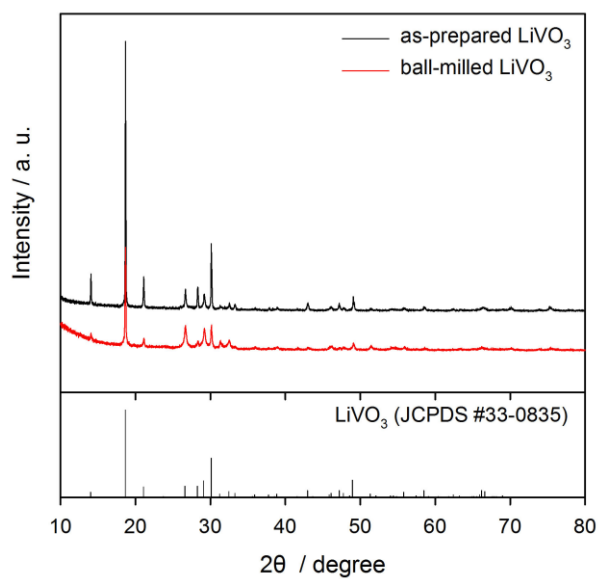
Figure S3. X-ray diffraction (XRD) of the synthesized LiVO$_3$. XRD patterns were measured with a Rigaku D/Max-3C diffractometer (Cu-Ka radiation source, $\lambda = 0.15418$ nm).
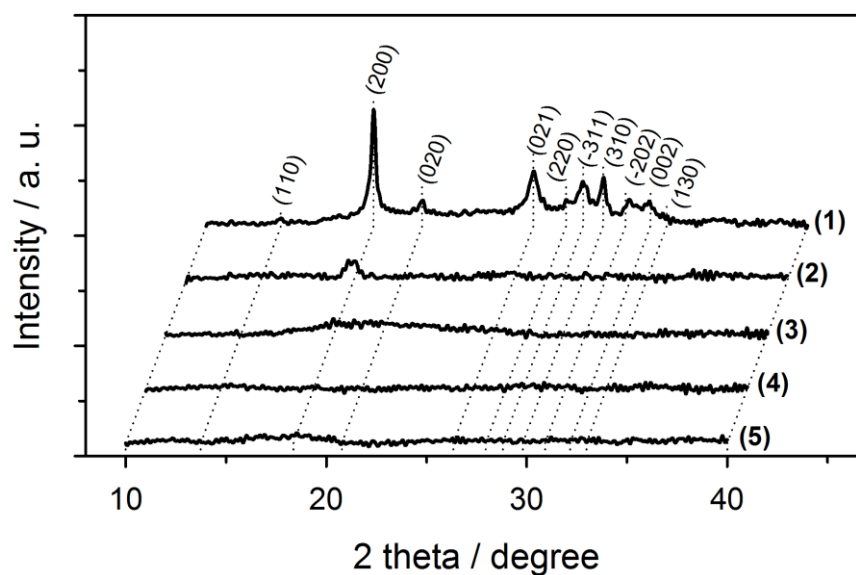
Figure S4. *Ex-situ* X-ray diffraction (XRD) of LiVO$_3$. The numbers indicate the points where the *ex-situ* XRD measurement were made in Figure 1. The cells were disassembled in an argon-filled dry glove box. XRD patterns were measured with a Rigaku D/Max-3C diffractometer (Cu-Ka radiation source, λ = 0.15418 nm). After the measurement, all XRD patterns were calibrated with the characterizing XRD peak of the Cu foil of the electrodes.

Li$_2$VO$_3$	E$_f$/[eV/VO$_3$]	Li$_2$VO$_3$	E$_f$/[eV/VO$_3$]	Li$_2$VO$_3$	E$_f$/[eV/VO$_3$]
Crystal70319	-41.2764	Crystal70398	-40.3891	Crystal70522	-40.7022
Crystal70325	-41.4002	Crystal70441	-40.8925	Crystal70529	-32.9432
Crystal70327	**-41.4009**	Crystal70450	-40.9967	Crystal70530	-39.2849
Crystal70346	-41.2089	Crystal70452	-40.7132	Crystal70532	-40.7115
Crystal70357	-41.3070	Crystal70455	-40.8973	Crystal70536	-41.0670
Crystal70359	-40.9351	Crystal70457	-41.2703	Crystal70540	-40.3409
Crystal70361	-41.0142	Crystal70484	-41.1338	Crystal70543	-41.0273
Crystal70364	-41.2618	Crystal70488	-41.2083	Crystal70544	-41.0581
Crystal70371	-40.7777	Crystal70499	-41.1523	Crystal70548	-41.3003
Crystal70392	-41.2092	Crystal70521	-40.3065		

Table S1. Formation energies of iso-structures of Li$_2$VO$_3$ phases obtained from ICSD and Materials project. Crystal70327, which is the most stable structure, corresponds to the structure of Li$_2$MnO$_3$ (ICSD-46953)
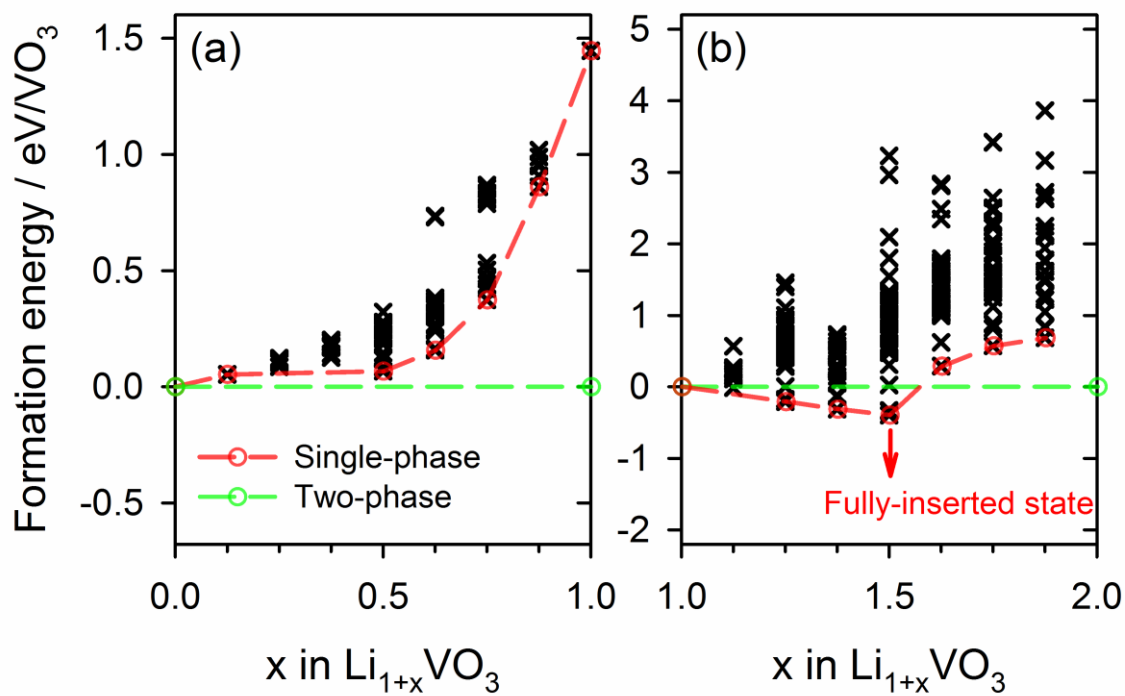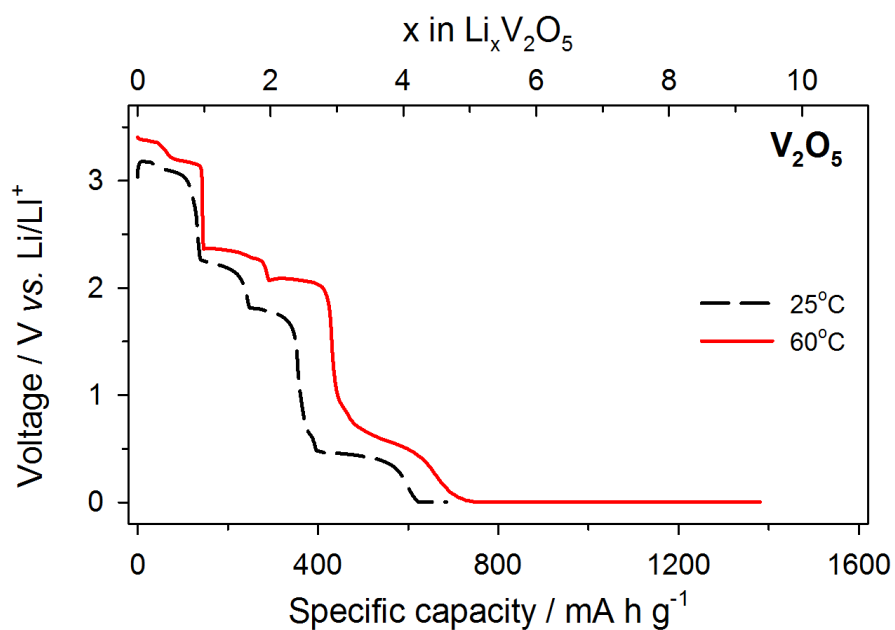
Figure S5. Formation energies of (a) single-phase reaction of $Li_{1+x}VO_3$ ($0 < x < 1$) compared with the two-phase reaction of $LiVO_3/Li_2VO_3$ and (b) single-phase reaction of $Li_{1+x}VO_3$ ($1 < x < 2$) compared with the two-phase reaction of Li_2VO_3/Li_3VO_3.
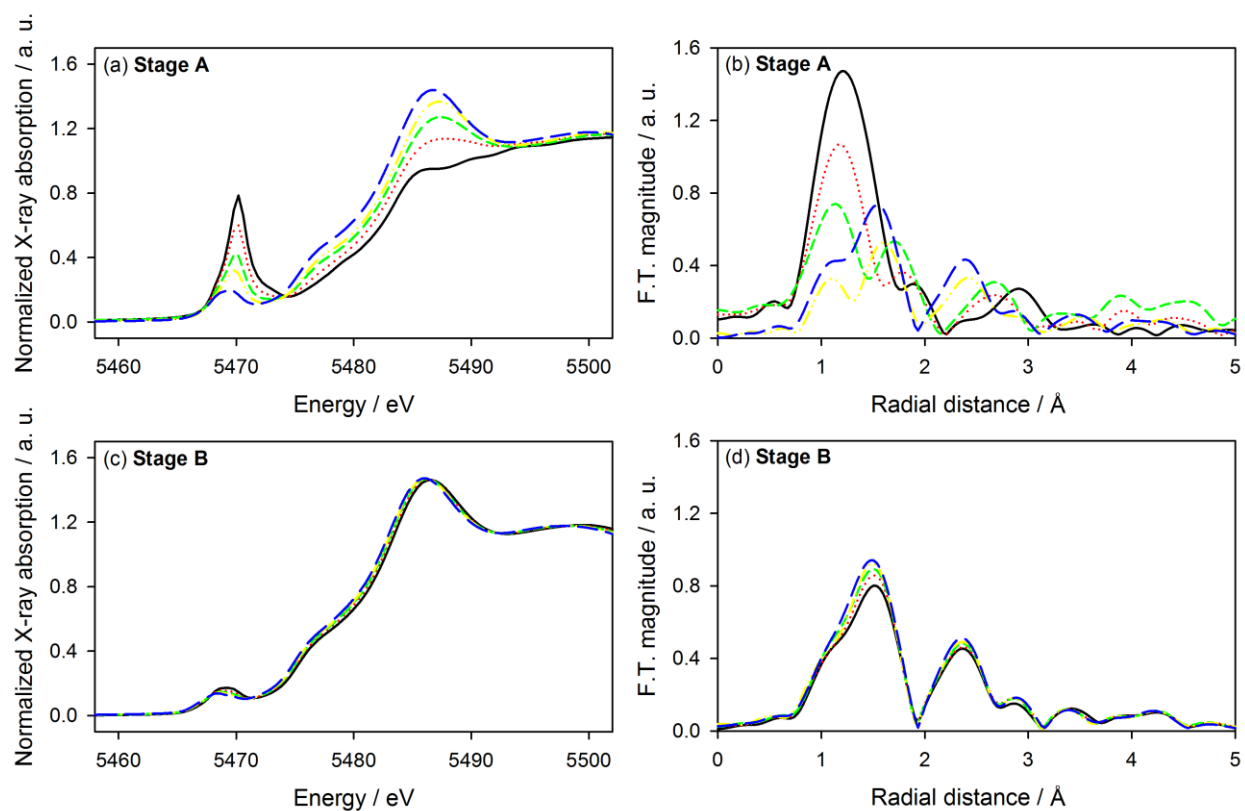
Figure S6. XANES and Fourier-transformed EXAFS spectra obtained during stage A (a), (b) and B (c), (d), respectively.

Figure S7. Galvanostatic lithiation voltage profiles of Li/V$_2$O$_5$ cell at 25°C and 60°C. The galvanostatic cycling was performed at a current density of 100 mA g^{-1} over the potential range of 0.005 – 3.0 V (vs. Li/Li$^+$) at 25°C and 60°C. Additional constant-voltage step was added at 0.005 V until the current decayed to 10 mA g^{-1}.
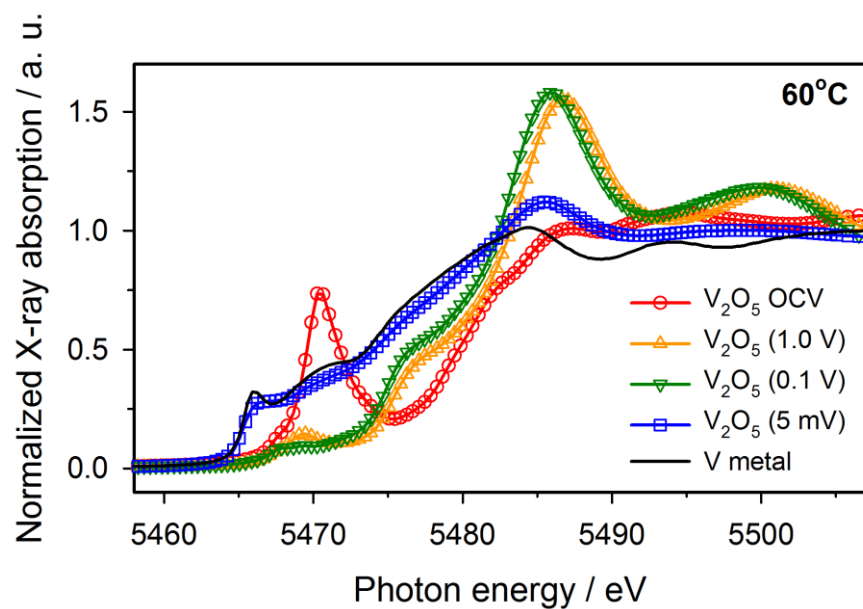
Figure S8. Normalized vanadium K-edge XANES spectra obtained from the V_2O_5 electrodes in the first lithiation period at 60°C.